

# Self-similar particle-size distributions during coagulation: theory and experimental verification

By JAMES R. HUNT

Division of Sanitary, Environmental, Coastal, and Hydraulic Engineering,  
University of California, Berkeley, California 94720

(Received 29 October 1980 and in revised form 24 March 1982)

A quantitative theory for particle coagulation in continuous particle size distributions is presented and experimentally verified. The analysis, following Friedlander (1960*a, b*), assumes a local equilibrium in the size distribution maintained by a particle flux through the size distribution. Only particle collisions caused by Brownian motion, fluid shear and differences in settling velocities are considered. For intervals of particle size where only one coagulation mechanism is dominant, dimensional analysis predicts self-similar size distributions that contain only one dimensionless constant for each mechanism. Experiments were designed to test these predictions with clay particles in artificial seawater sheared in the gap between concentric rotating cylinders. Particle-size distributions measured over time were self-similar in shape and agreed with the Brownian- and shear-coagulation prediction in terms of shape and dependence on fluid shear rate and particle volume flux through the size distribution.

---

## 1. Introduction

In many industrial processes, particle removal from fluids is important because either the particles contain important minerals which are being concentrated, or the particles are pollutants that must be removed before effluent discharge. The particles of interest are typically very small and cannot be separated over reasonable time periods by quiescent settling. To accelerate suspended-particle removal, particles are coagulated or aggregated into larger particles that have greater settling velocities and can be separated from the fluid in reasonable time periods. Particle coagulation is also important in controlling the removal of suspended particles from natural waters, especially estuaries and coastal waters.

A fundamental understanding of particle coagulation has been limited to the initial coagulation kinetics of particles uniform in size. These results cannot be applied quantitatively to suspensions containing continuous distributions of particle sizes as are commonly encountered. Because of the lack of a verified theory for coagulation in continuous particle-size distributions, design of particle-separation systems involving coagulation and settling has been empirical and dependent on extensive pilot plant studies. This paper presents a theoretical derivation of coagulating particle-size distributions extending results obtained earlier by Friedlander (1960*a, b*). The approach, valid after sufficient time, assumes that the particle-size distribution is in local equilibrium maintained by a flux of particles through the size distribution. The size-distribution predictions for Brownian and shear coagulation are verified experimentally with clay particles in artificial seawater.

*Coagulation mechanisms*

A continuous distribution of particle sizes is represented by a size distribution function  $n(v)$  distributed on particle volume  $v = \frac{1}{6}\pi d_p^3$ , where  $d_p$  is the particle diameter. The number concentration  $dN$  of particles in a small interval  $dv$  of particle volume is given by

$$dN = n(v) dv. \quad (1.1)$$

The dimensions of  $n(v)$  are number of particles per volume of fluid per particle-volume interval, represented as  $[L^{-3}l^{-3}]$ , where  $[L]$  is a fluid-length unit and  $[l]$  is a particle-length unit. Particle-size distributions in terms of volume are convenient for discussion of coagulation theory since particle volume is conserved during coagulation.

A general equation describing a particle-size distribution undergoing coagulation and settling is (see Friedlander 1977)

$$\frac{\partial n(v)}{\partial t} = \frac{1}{2} \int_0^v \beta(\bar{v}, v - \bar{v}) n(\bar{v}) n(v - \bar{v}) d\bar{v} - \int_0^\infty \beta(v, \bar{v}) n(v) n(\bar{v}) d\bar{v} - \frac{g(\rho_p - \rho_f)}{18\mu} \left(\frac{6}{\pi}\right)^{\frac{2}{3}} v^{\frac{2}{3}} \frac{\partial n(v)}{\partial z}, \quad (1.2)$$

where the dependence of the size distribution on vertical position  $z$ , positive downward, and time  $t$  was not indicated explicitly. In (1.2) the first term on the right-hand side represents the collision of particles producing a particle volume  $v$ , where  $\beta(\bar{v}, v - \bar{v})$  is a collision-frequency function for particles of volume  $\bar{v}$  colliding with particles of volume  $v - \bar{v}$  by all coagulation mechanisms. The second term is the removal of particles of volume  $v$  by coagulation with all particles. Particle removal by settling using Stokes' equation is represented by the third term, where  $g$  is the gravitational acceleration,  $\mu$  the fluid viscosity,  $\rho_p$  the particle density, and  $\rho_f$  the fluid density.

In this study three coagulation mechanisms are considered, each with a collision function represented below for collisions between particles of volumes  $v_i$  and  $v_j$ . For collisions arising from the Brownian or thermal motion of particles, Smoluchowski (1917) showed that

$$\beta_b(v_i, v_j) = \frac{2kT}{3\mu} \frac{(v_i^{\frac{1}{3}} + v_j^{\frac{1}{3}})^2}{v_i^{\frac{1}{3}} v_j^{\frac{1}{3}}}, \quad (1.3)$$

where  $k$  is the Boltzmann constant, and  $T$  the absolute temperature. If a fluid is sheared in laminar flow, particles moving with the fluid collide, and the collision functions for shear coagulation are (as also shown by Smoluchowski 1917)

$$\beta_{sh}(v_i, v_j) = \frac{G}{\pi} (v_i^{\frac{1}{3}} + v_j^{\frac{1}{3}})^3, \quad (1.4)$$

where  $G$  is the fluid shear rate or mean-velocity gradient.

Smoluchowski arrived at the Brownian- and shear-coagulation collision functions assuming geometrical collisions unhindered by hydrodynamic, electrostatic or van der Waals forces during collision (see Friedlander 1977). Corrections for these forces have been obtained when spheres of equal size collide by Brownian motion (Spielman 1970; Honig, Roeberson & Wiersema 1971) and by fluid shear (van de Ven & Mason 1977; Zeichner & Schowalter 1977). For the collision of spheres of unequal size, techniques are available to calculate collision efficiencies which include hydrodynamic, electrostatic, and van der Waals forces (Adler 1981). The theoretical results of Adler (1981) and experimental data of Manley & Mason (1955) indicate that hydrodynamic forces

greatly limit shear-induced collisions when the colliding particles differ by a factor of two or more in diameter.

The third coagulation mechanism occurs when a faster-settling particle overtakes and collides with a slower-settling particle. The collision function for differential-sedimentation coagulation is the collision cross-section times the difference in particle Stokes settling velocities, assuming a constant particle density

$$\beta_{ds}(v_i, v_j) = \left(\frac{6}{\pi}\right)^{\frac{2}{3}} \frac{\pi g(\rho_p - \rho_f)}{72\mu} (v_i^{\frac{2}{3}} + v_j^{\frac{2}{3}})^2 |v_i^{\frac{2}{3}} - v_j^{\frac{2}{3}}|. \quad (1.5)$$

Hydrodynamic forces are known to limit the collision efficiency of this mechanism for water droplets in air (Mason 1971), but corrections for hydrodynamic, electrostatic and van der Waals forces are not available for particles suspended in water. In the collection of particles on filter media these forces are important in determining the collection efficiency (Spielman 1977).

## 2. Previous solutions for coagulating suspensions

This section reviews previous predictions for particle coagulation kinetics. Equation (1.2) can be simplified if a suspension contains particles all of the same size, that is a monodisperse suspension, which will exist only for small times after coagulation has begun. Other methods predict the dynamics of continuous particle-size distributions for various coagulation mechanisms, with and without removal by settling.

For a monodisperse suspension, coagulation kinetics are straightforward if settling is neglected (Friedlander 1977). If coagulation is by Brownian motion only, (1.2) can be reduced to a second-order rate equation in total particle concentration. Experimentally observed coagulation rates are less than the theoretical rate, with the discrepancy explained by the influence of hydrodynamic and van der Waals forces (Lichtenbelt, Pathmamanoharan & Wiersema 1974). Experiments were conducted in solutions of high ionic strength, which eliminated electrostatic forces between particles.

In a monodisperse, non-settling suspension dominated by shear coagulation, (1.2) becomes a first-order rate equation in total particle concentration. The rate expression has been verified by Swift & Friedlander (1964) in laminar shear flow and by Birkner & Morgan (1968) in turbulent flow. Again, corrections for hydrodynamic and van der Waals forces explained the difference between observed and theoretical rates (van de Ven & Mason 1977; Zeichner & Schowalter 1977). In a monodisperse suspension differential sedimentation coagulation is not expected to occur because  $\beta(v_i, v_i) = 0$ .

These results for monodisperse suspensions are not applicable to the analysis of coagulation in suspensions containing a broad distribution of particle sizes. There have been two approaches to solving (1.2) for a continuous particle-size distribution, using either direct numerical solutions or asymptotic solutions for later times by a self-preserving transformation. Two recent examples of direct numerical solutions are those of Gelbard & Seinfeld (1979) for aerosol dynamics and Lawler, O'Melia & Tobiason (1980) for hydrosol dynamics. These numerical solutions have not been verified with experimental data.

Partial solutions to (1.2) have been obtained by self-preserving transformations. Friedlander (1960*b*) showed that a self-preserving transformation reduced the equation

for Brownian coagulation and settling from a partial integro-differential equation to an ordinary integro-differential equation. The general shear-coagulation equation also had a self-preserving transformation, and experimentally measured size distributions of coagulating hydrosols and emulsions approached a self-preserving distribution after sufficient time (Swift & Friedlander 1964). A self-preserving transformation also existed for simultaneous Brownian and shear coagulation only if the shear rate over time was proportional to the total number of particles (Wang & Friedlander 1967). Pulvermacher & Ruckenstein (1974) and Drake (1976) have discussed the existence of self-preserving solutions for a number of coagulation mechanisms.

The concept of a self-preserving transformation of (1.2) has had considerable utility in aerosol-coagulation studies, but the application to hydrosols is limited. For aerosols, Brownian coagulation is usually the dominant mechanism for larger aerosol growth, while, for hydrosols, Brownian and shear coagulation are known to be important, and possibly also coagulation by differential sedimentation. Thus, for hydrosols, all coagulation mechanisms must be considered, and the restriction necessary for a self-preserving transformation, that the shear rate is proportional to the particle concentration, is not a general result with wide application. Quantitative application of the self-preserving transformation also requires corrections to the collision functions for hydrodynamic, electrostatic and van der Waals forces.

### 3. Self-similar solutions for coagulation

A general solution to (1.2) will not be attempted; instead self-similar solutions are obtained dimensionally after considerable simplification. The approach is an extension of that of Friedlander (1960*a, b*), where Brownian coagulation and settling of atmospheric aerosols were considered. Friedlander's analysis is directly analogous to previous work in the universal equilibrium spectra of turbulent variations in velocity and scalar fields (Batchelor 1953, 1959).

Four assumptions are required in the analysis of coagulating particle distribution. The first, and major, limiting assumption is that the particle distribution is in a dynamic steady state, or equilibrium. There is an assumed source of small particles, which coagulate through the size distribution to an aggregate size large enough for removal by settling. For a small interval of particle size there is a balance between the particle volume coagulating into that interval and the volume lost from the interval by coagulation. The existence of a dynamic steady-state distribution maintained by a volume flux through the distribution limits the application of the results to long times after the start of particle coagulation. The volume flux is denoted by  $E$ , with dimensions  $[L^3L^{-3}t^{-1}]$ , where  $[t]$  is the time unit.

The second assumption is that only one coagulation mechanism is dominant at a given particle size. To show the strict validity of this assumption would require demonstrating that the contribution to the volume flux at a given particle size is dominated by particle collisions near that size, and also that only one mechanism is significant at that size. The coagulation collision functions given in (1.3)–(1.5) imply that collisions are possible between particles of all sizes if various fluid and particle forces are not considered. For Brownian coagulation, the influence of hydrodynamic forces on the collision of unequal spheres could be obtained following Spielman (1970), but no calculations or data are available to estimate the influence of hydro-

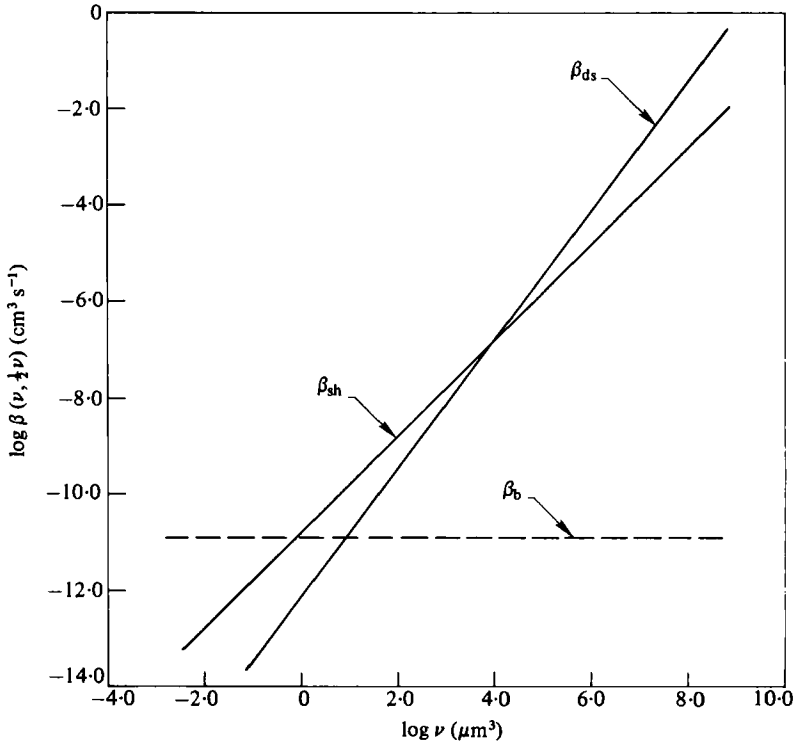


FIGURE 1. Comparison of Brownian, shear and differential-sedimentation coagulation collision functions in water for particles of volume  $v$  colliding with particles of volume  $\frac{1}{2}v$ ; assuming  $T = 25^\circ\text{C}$ ,  $G = 8\text{ s}^{-1}$ ,  $\rho_p - \rho_t = 0.1\text{ g cm}^{-3}$  and  $\mu = 0.89 \times 10^{-2}\text{ g cm}^{-1}\text{ s}^{-1}$ .

dynamic forces on hindering the collision between unequal spheres. For shear and differential-sedimentation coagulation, hydrodynamic forces hinder collision between particles different in size. Based on the limited information, collisions between particles much-different in size can be assumed to have little contribution to the volume flux through the distribution.

Considering collisions only between particles comparable in size, regions exist where only one coagulation mechanism is dominant. In figure 1 the coagulation collision functions in (1.3)–(1.5) are plotted individually for particles of size  $v$  colliding with particles of size  $\frac{1}{2}v$  for indicated values of temperature, fluid shear rate and particle density. Under these conditions, collisions of a particle and another one-half its volume occur most frequently by Brownian motion for  $v < 10^{-1}\mu\text{m}^3$ , shear coagulation causes the greatest number of collisions for  $10\text{--}10^3\mu\text{m}^3$  particles, and for  $v > 10^5\mu\text{m}^3$  differential-sedimentation coagulation is the dominant collision mechanism. Other choices of the ratio of colliding particle volumes, fluid shear rates and particle density would shift the curves but still retain the regions of dominance: Brownian at the smallest volumes, shear at intermediate sizes, and differential sedimentation coagulation at larger volumes. Particle removal by gravitational settling cannot be compared with the coagulation mechanisms in this plot, but it is reasonable that gravitational settling is dominant for the largest particles.

The third assumption is that the efficiency of particle sticking on collision is

independent of particle size. Most particles suspended in water are charged, and electrostatic repulsive forces exist between particles. At sufficiently high concentration of ions in solution, the electrostatic forces are masked and attractive van der Waals forces cause the sticking of particles. Overbeek (1977) reviews current problems in understanding suspended-particle stability at lower ionic strengths when electrostatic forces exist and collision efficiency may be a function of particle size.

The fourth assumption is that each coagulation mechanism can be characterized by a single parameter. The coagulation parameters and associated dimensions for Brownian, shear and differential-sedimentation coagulation are obtained from (1.3)–(1.5) respectively, and the parameters are chosen to be independent of particle size:

$$\text{Brownian} \quad K = kT/\mu \quad [L^3t^{-1}]; \quad (3.1)$$

$$\text{shear} \quad G \quad [L^3l^{-3}t^{-1}]; \quad (3.2)$$

$$\text{differential sedimentation} \quad S = g(\rho_p - \rho_t)/\mu \quad [L^3l^{-4}t^{-1}]. \quad (3.3)$$

With these assumptions the particle-size distribution has the functional form

$$n = n(v, E, K, G, S). \quad (3.4)$$

Selecting an interval of particle volume where only one coagulation mechanism is dominant, (3.4) becomes an expression in four variables and three units ( $l$ ,  $L$  and  $t$ ). The following size distributions are obtained dimensionally:

$$\text{Brownian} \quad n(v) = A_b \left( \frac{E}{K} \right)^{\frac{1}{2}} v^{-\frac{3}{2}}; \quad (3.5)$$

$$\text{shear} \quad n(v) = A_{sh} \left( \frac{E}{G} \right)^{\frac{1}{2}} v^{-2}; \quad (3.6)$$

$$\text{differential sedimentation} \quad n(v) = A_{ds} \left( \frac{E}{S} \right)^{\frac{1}{2}} v^{-\frac{3}{2}}. \quad (3.7)$$

Here  $A_b$ ,  $A_{sh}$  and  $A_{ds}$  are dimensionless constants. Friedlander's (1960*a, b*) analysis of coagulating and settling aerosol size distributions arrived at the Brownian prediction in (3.5) and a prediction for gravitational-settling dominance. The settling prediction has been criticized by Pruppacher & Klett (1978) as not being physically based because the vertical gradient in particle concentration was neglected. Jeffrey (1981) has rederived the above results based on the particle volume flux through the distribution and has considered a range where settling and coagulation both occur.

The predictions in (3.5)–(3.7) are in reasonable agreement with particle-size distributions observed in oceanic waters. These predictions also appear to account for the maximum in particle concentration that has been frequently observed in the oceanic thermocline, as clearly there is a decreased rate of fluid shear in the thermocline (Hunt 1980*b*).

#### 4. Experimental procedures for testing predictions

This section summarizes the experimental procedures for testing the Brownian- and shear-coagulation predictions. With the instrumentation available for measuring particle-size distributions, larger aggregates could not be sized, and the differential-sedimentation coagulation prediction was not tested. Hunt (1980*a*) contains a more complete description of experimental procedures.

##### *Data presentation and normalization*

Number distributions  $n(v)$  are measured experimentally, but they are not the best method for graphically presenting the experimental data described by the Brownian- and shear-coagulation predictions in (3.5) and (3.6). A more convenient form for representation of size-distribution data is a volume distribution  $dV/d(\log d_p)$ , which is the suspended particle volume in a logarithmic interval of particle diameter, and is related to the number distribution by (see Friedlander 1977)

$$\frac{dV}{d(\log d_p)} = \frac{2 \cdot 3 \pi^2}{12} d_p^3 n(v), \quad (4.1)$$

where 2.3 is  $\log_e 10$ . Here the total suspended-particle volume concentration  $V$  is related to the size distribution by

$$V = \int_0^\infty vn(v) dv. \quad (4.2)$$

For aqueous suspensions, the volume distribution and total suspended-particle volume are reported in units of parts per million by volume (1 p.p.m. by volume =  $10^{-6}$  cm<sup>3</sup>/ml). Predicted volume distributions for Brownian and shear coagulation become

Brownian 
$$\frac{dV}{d(\log d_p)} = 5 \cdot 0 A_b \left( \frac{E}{K} \right)^{\frac{1}{2}} d_p^{\frac{3}{2}}, \quad (4.3)$$

shear 
$$\frac{dV}{d(\log d_p)} = 6 \cdot 9 A_{sh} \left( \frac{E}{G} \right)^{\frac{1}{2}}. \quad (4.4)$$

Experiments were designed to test the dependence of the volume distribution on particle diameter, particle volume flux  $E$ , and fluid shear rate  $G$ . A convenient way to present the data and to test the agreement with predictions is to normalize or scale the data such that all volume distributions are represented by a single distribution. Particle diameters are normalized by the characteristic diameter that separates Brownian-coagulation dominance from shear-coagulation dominance. The particle diameter where Brownian and shear coagulation have equal collision frequency is found by equating (1.3) and (1.4) for  $v_i = v_j$ , giving a particle volume of  $\pi kT/3\mu G$ , corresponding to a diameter of  $(2kT/\mu G)^{\frac{1}{2}}$  or  $(2K/G)^{\frac{1}{2}}$ . A normalized particle diameter  $\delta$  is defined as

$$\delta = d_p \left( \frac{G}{K} \right)^{\frac{1}{2}}. \quad (4.5)$$

with the property that Brownian coagulation is expected to be dominant for  $\delta \ll 2^{\frac{1}{2}}$  and shear coagulation for  $\delta \gg 2^{\frac{1}{2}}$ . The normalized diameter is proportional to the cube root of a Péclet number  $Pe = Gd_p^3/D$ , where  $D = kT/3\pi\mu d_p$ , the Stokes-Einstein

expression for particle diffusivity. The Péclet number is the ratio of fluid-shear particle-mass transport to diffusive mass transport.

The normalized volume distribution  $d\bar{V}/d(\log \delta)$  is taken as

$$\frac{d\bar{V}}{d(\log \delta)} = \frac{dV}{d(\log d_p)} \left(\frac{G}{\bar{E}}\right)^{\frac{1}{2}}, \quad (4.6)$$

which, combined with (4.5), transforms the Brownian- and shear-coagulation predictions into

$$\text{Brownian} \quad \frac{d\bar{V}}{d(\log \delta)} = 5.0A_b \delta^{\frac{3}{2}}, \quad (4.7)$$

$$\text{shear} \quad \frac{d\bar{V}}{d(\log \delta)} = 6.9A_{sh}. \quad (4.8)$$

With this normalization procedure, all experimental data in agreement with the Brownian- and shear-coagulation predictions should collapse onto a single curve described by (4.7) for  $\delta \ll 2^{\frac{1}{2}}$  and (4.8) for  $\delta \gg 2^{\frac{1}{2}}$ .

#### *Experimental methods*

The purpose of the experiments is to test the predicted size-distribution dependence on diameter, fluid shear rate, and volume flux. This section describes the aqueous and solid media, the particle-sizing technique, and the use of batch coagulation experiments.

All experiments were conducted in artificial seawater prepared according to a recipe of Lyman and Fleming from Riley & Skirrow (1965). Background suspended particles were removed from the artificial seawater by 0.22  $\mu\text{m}$  Millipore filtration. Experiments were performed at room temperature (22–24 °C) with suspended-particle volume concentration less than 0.1 %, which fixed the value of the Brownian coagulation parameter  $K = kT/\mu = 4.38 \times 10^{-12} \text{ cm}^3 \text{ s}^{-1}$ .

Clay minerals were selected for the testing of the predictions because of their presence in natural waters and the importance of clay-particle surfaces in transporting adsorbed pollutants. The clays were obtained from Ward's Natural Science Establishment Inc., and were representative of clay minerals previously characterized by the American Petroleum Institute (Kerr *et al.* 1949–50). Kaolinite (A.P.I. no. 35) was from Oneal Pit, Macon, Georgia, U.S.A., and illite (A.P.I. no. 35) was from Fithian, Illinois, U.S.A. Clay particles are not spherical but consist of negatively charged flat sheets with positively charged edges. Illite clay particles have a greater surface charge density than kaolinite particles because of a greater cation-exchange capacity. Crushed clay particles were cleaned and the clay surfaces were converted to their sodium form following procedures recommended by van Olphen (1977). The clay suspensions were allowed to settle quiescently to remove particles greater than 2  $\mu\text{m}$  equivalent spherical diameter. Edzwald, Upchurch & O'Melia (1974) observed that the ionic strength of seawater was sufficient to destabilize clay particles.

Aggregate size distributions were measured with a Model ZBI Coulter Counter interfaced with a Nuclear Data logarithmic amplifier and multichannel analyser. The Coulter Counter counts and sizes aggregates by pulling aggregates, one at a time, through a small aperture and measuring the change in electrical resistance across the aperture. The resistance change is proportional to the particle volume, and the instrument is able to count and size suspended particles.

In the theoretical development, the volume flux through the distribution was assumed to be a constant, resulting in a local equilibrium in the particle-size distribution. Such a system could only be obtained by continuously adding very small particles and turbulently mixing those small particles throughout the reactor volume. There are two problems with using turbulent flow for these experiments. First, low levels of fluid shear are required to observe Brownian-coagulation dominance with the sizing instrument limited to particle diameters greater than  $0.6\ \mu\text{m}$ . Secondly, turbulent flow has a distribution of fluid shear rates about a mean value. Because particle aggregates are weak, localized high-intensity fluid shear could disrupt aggregates, which is not a mechanism under consideration. An experimental test of the Brownian- and shear-coagulation size-distribution predictions required batch experiments with uniform fluid shear, resulting in decaying particle-size distributions rather than steady-state distributions. In batch experiments the particle volume flux decreased with time.

To control the fluid-shear rate, the suspension was sheared in the gap between two concentric rotating cylinders, which gave a well-defined mean shear rate with little variation about the mean. The apparatus was aligned vertically to allow larger aggregates to settle. With a fixed inner cylinder of  $7.5\ \text{cm}$  diameter and a gap width of  $0.63\ \text{cm}$ , shear rates of  $0.5\text{--}32\ \text{s}^{-1}$  were possible. Experimental evidence indicated that a fluid instability occurred at  $32\ \text{s}^{-1}$ , probably caused by cylinder surface roughness. Taylor's (1936) experiments with a similar cylinder diameter and gap width developed instabilities at a shear rate of  $250\ \text{s}^{-1}$ .

An experiment was started by rapidly mixing  $2\ \text{ml}$  of concentrated clay suspension with  $200\ \text{ml}$  of filtered artificial seawater in a  $250\ \text{ml}$  beaker. The destabilized suspension was then poured into the gap of the rotating-cylinder apparatus. The initial particle volume concentration for all kaolinite experiments was  $276\ \text{p.p.m.}$  by volume, and was  $90\ \text{p.p.m.}$  by volume for all illite experiments. Using high initial clay-particle concentrations and waiting  $10\text{--}25\ \text{min}$  before withdrawing the first sample assured the establishment of a local equilibrium in the coagulating particle-size distribution. Samples were withdrawn one to four centimetres below the surface through a piece of flexible Tygon tubing into a graduated pipette. The minimum bore diameter was  $0.3\ \text{cm}$  and withdrawal flow rates were less than  $0.5\ \text{mls}^{-1}$ ; these procedures were adopted to minimize aggregate disruption.

During batch experiments in local equilibrium, the rate of decrease in total suspended-particle volume is nearly equal to the particle volume flux through the distribution or

$$-\frac{dV}{dt} = E(t). \quad (4.9)$$

$E(t)$  can be related back to  $V(t)$  by noting that  $V(t)$  is related to  $n(v, t)$  by (4.2) and that  $n(v, t)$  is proportional to  $E^{\frac{1}{2}}(t)$  from coagulation predictions in (3.5)–(3.7). Thus  $V(t) \propto E^{\frac{1}{2}}(t)$ , or

$$E(t) = bV^2(t), \quad (4.10)$$

where  $b$  is a removal-rate parameter dependent on the coagulation parameters. Equations (4.9) and (4.10) and experimental data indicate that total suspended-particle volume decay rate is second order in suspended volume, or

$$V(t) = \frac{1}{a + bt}, \quad (4.11)$$

where  $a$  is a constant. Equation (4.10) was used to estimate instantaneous particle volume flux, with the value of  $b$  obtained experimentally from the slope of an inverse-volume plot with time, as in (4.11).

Calculation of the particle volume flux from (4.10) overestimates the Brownian- and shear-coagulation volume flux for batch experiments. From (1.2), particle coagulation is second order in number concentration and particle removal by settling is first order in the gradient of the number concentration. During a batch experiment where coagulation and settling occur, the particle-size interval dominated by coagulation is expected to decrease with time as the particle concentration decreases. This shift in coagulation dominance away from larger sizes causes a loss of particle volume both by the coagulation flux through the distribution and loss by settling of smaller and smaller particles.

Since the sizing instrument broke up larger aggregates, the total suspended volume could not be obtained from the measured particle-size distribution. Total suspended volume was determined from suspension optical absorbance, which is a measure of the light scattered by the suspended particles. Absorbance of a shaken suspension at low concentration was proportional to total suspended volume. Absorbance measurements were made with a 1 cm or a 5 cm optical cell, depending on the suspension concentration.

## 5. Experimental results and discussion

The predicted size distributions for Brownian and shear coagulation were verified for kaolinite and illite clay particles sheared in artificial seawater. This section only summarizes the results, which are presented in detail in Hunt (1980a).

### *Kaolinite*

Because of larger aggregate breakup during counting, valid kaolinite-aggregate size distributions were measured only for diameters from 0.6 to 1.2  $\mu\text{m}$ . Figure 2 is an example of larger aggregate breakup during counting for one sample of kaolinite aggregates sized with 30, 70 and 140  $\mu\text{m}$  diameter Coulter Counter apertures. The sample was withdrawn after 35 minutes of shearing at 4  $\text{s}^{-1}$ . The settings of the Coulter Counter were chosen to measure the smallest aggregates possible with each aperture such that the counts recorded for a sample were always ten times greater than the counts recorded in a blank solution. The lack of alignment in volume distributions between apertures in their regions of diameter overlap was caused by aggregate breakup during passage through the apertures where flow rates and fluid shear are high. The problem of larger aggregate breakup existed during all coagulation experiments with solid particles.

Kaolinite coagulation experiments were conducted at shear rates of 1, 2, 4, 8, 16 and 32  $\text{s}^{-1}$ . At each shear rate the reciprocal of the total suspended volumes, plotted in figure 3, were linear with time, as was asserted in (4.11). The slopes of the lines, which are the second-order removal-rate constants, increased with shear rate to a maximum at 16  $\text{s}^{-1}$ . The volume removal rate declined at  $G = 32 \text{ s}^{-1}$  because of a fluid instability. The instantaneous volume fluxes through the distribution were estimated from (4.10).

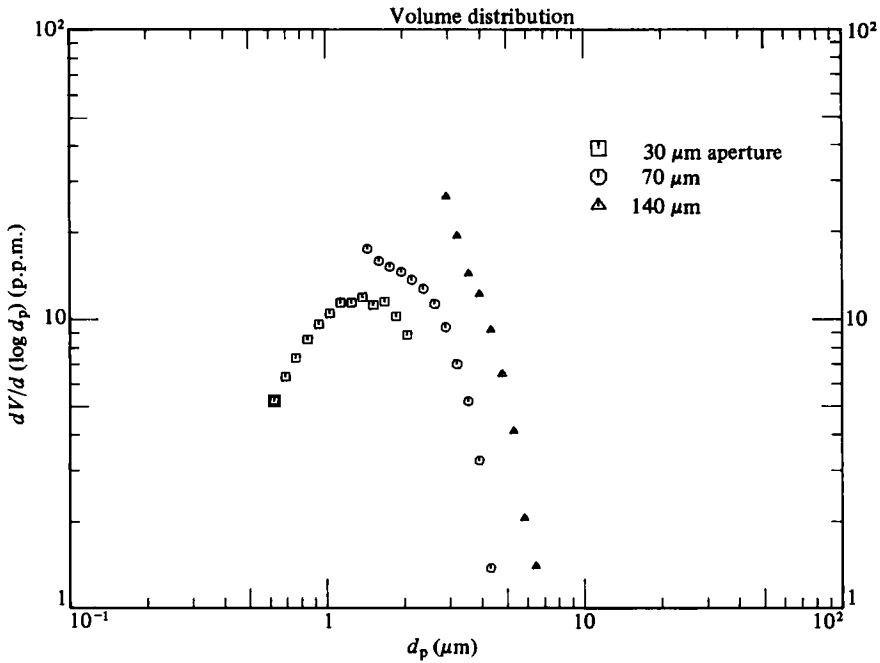


FIGURE 2. Volume distributions of kaolinite after 35 minutes of shearing at  $G = 4 \text{ s}^{-1}$  measured by 30, 70 and 140  $\mu\text{m}$  apertures.

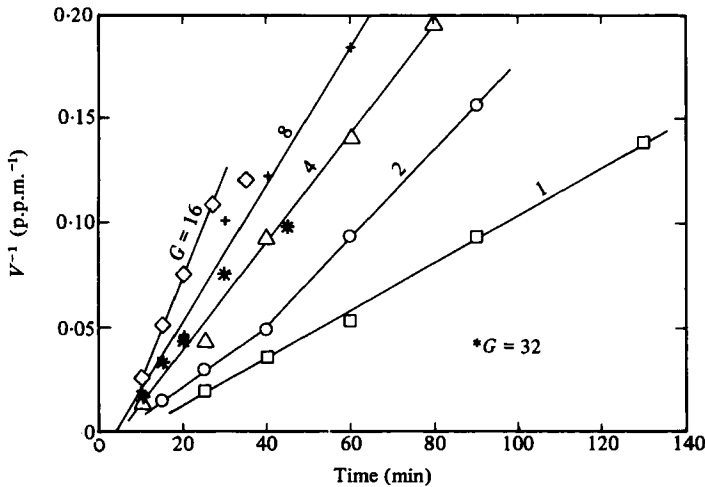


FIGURE 3. Inverse total suspended-particle volume during kaolinite experiments at shear rates of 1, 2, 4, 8, 16 and 32  $\text{s}^{-1}$ .

Volume distributions and normalized volume distributions are given in figure 4 for a fluid shear rate of  $1 \text{ s}^{-1}$ . The volume distributions measured during the batch experiment had the same shape, only shifted downward with time. This local equilibrium in the size distribution indicates that a steady-state size distribution was a valid assumption. Normalization of diameters and volume distributions reduced the vertical spread, and a line of slope  $\frac{3}{2}$ , the Brownian prediction, fits the trend of the data. No region of

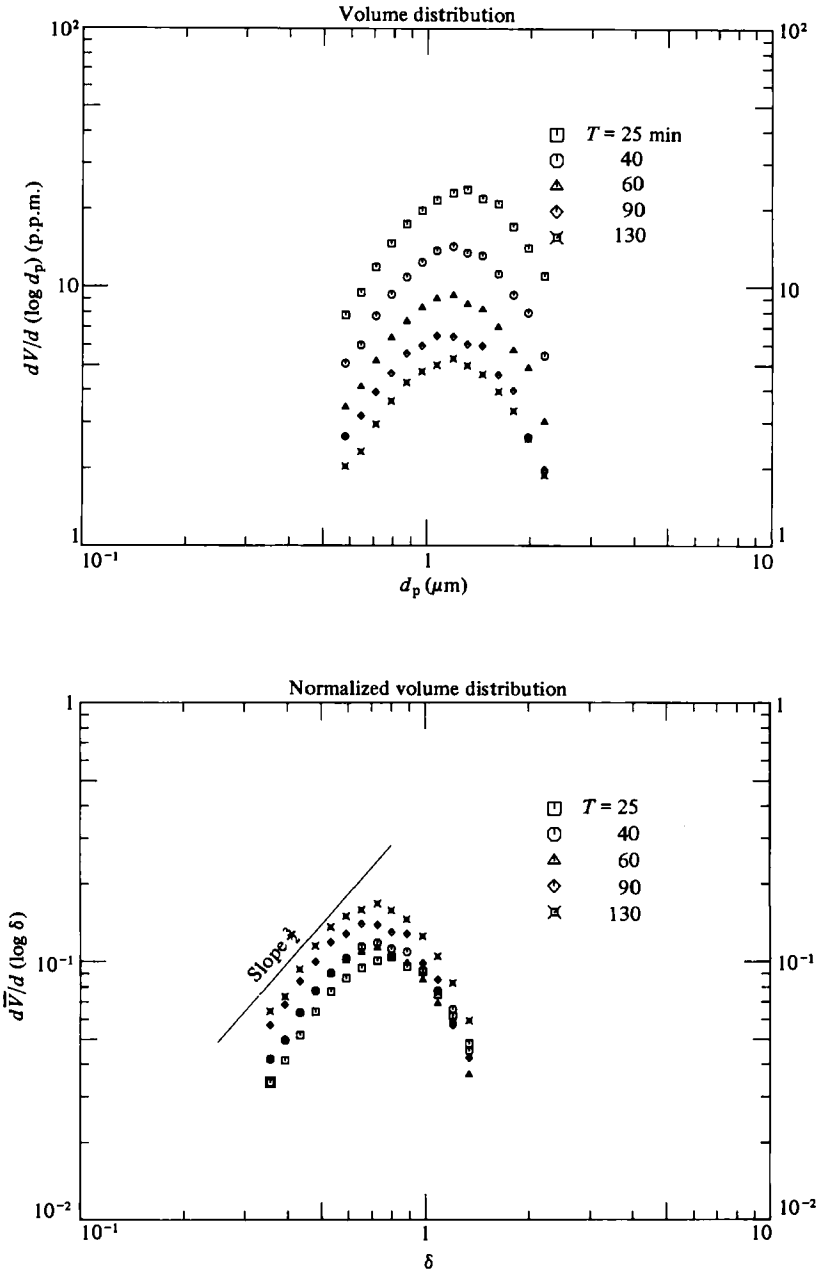


FIGURE 4. Volume distributions and normalized volume distributions for kaolinite at  $G = 1 \text{ s}^{-1}$ .

possible shear-coagulation dominance was observed at this shear rate because larger aggregates were broken up during the counting process.

Volume distributions measured over time at shear rates of 2, 4, 8, 16 and  $32 \text{ s}^{-1}$  also achieved self-similar distributions, which were reduced in spread on normalization. According to (4.7) and (4.8), normalized volume distributions measured at all shear

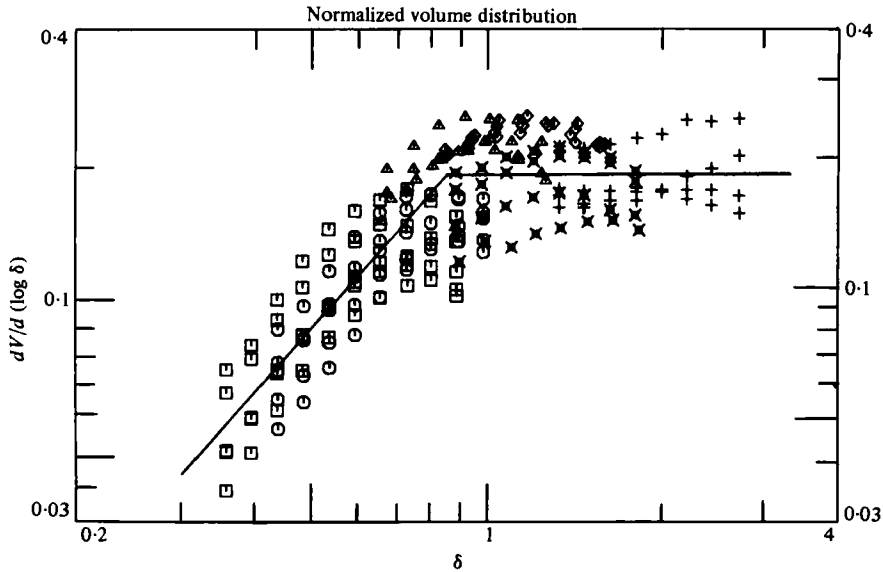


FIGURE 5. Normalized distributions for kaolinite in seawater at  $G = 1$  ( $\square$ ),  $2$  ( $\circ$ ),  $4$  ( $\triangle$ ),  $8$  ( $\diamond$ ),  $16$  ( $\times$ ) and  $32$   $s^{-1}$  ( $+$ ).

rates and volume fluxes should fall on a single curve. The agreement between the kaolinite data and the predictions was tested in figure 5, where all normalized kaolinite data were plotted, excluding the larger-aggregate data at each shear rate dominated by breakup during counting. A line of slope  $\frac{2}{3}$ , the Brownian prediction, fits the trend of the data for  $\delta < 0.9$ , and a level line, the shear prediction, fits the data for  $\delta > 0.9$ . The vertical spread in the normalized data present at each shear rate is caused by the overestimation of the volume flux from the total suspended volume removal rate. The dimensionless coagulation constants are estimated to be  $A_b = 0.046$  and  $A_{sh} = 0.026$ .

#### Illite

Experiments were conducted with illite in seawater at shear rates of  $\frac{1}{2}$ ,  $1$ ,  $2$ ,  $4$ ,  $8$ ,  $16$  and  $32 s^{-1}$ . Inverse total suspended volumes measured during batch experiments are plotted in figure 6, and the data indicate that the maximum removal-rate constant occurred at  $8 s^{-1}$ . A fluid instability prevented the removal of suspended volume during the experiment at  $G = 32 s^{-1}$ .

Volume distributions measured during each illite experiment were self-similar in shape and the vertical spread was substantially reduced on normalization. Figure 7 is a plot of the normalized data for shear rates from  $0.5$  to  $16 s^{-1}$ , including only that portion of the distributions not dominated by aggregate breakup during counting. In the plot a line of slope  $\frac{2}{3}$  and a level line were drawn by eye and fit the trend of the data. The vertical spread in the normalized data is less than that observed for kaolinite, and unlike kaolinite the separation between Brownian- and shear-coagulation dominance occurs at about  $\delta = 0.44$ . The normalized data for  $G = 16 s^{-1}$  are above the trend of the other data, and, combined with the decreased volume removal rate shown in figure 6, indicate that aggregate breakup in the rotating-cylinder apparatus was occurring at this shear rate. At  $G = 32 s^{-1}$  the volume distributions

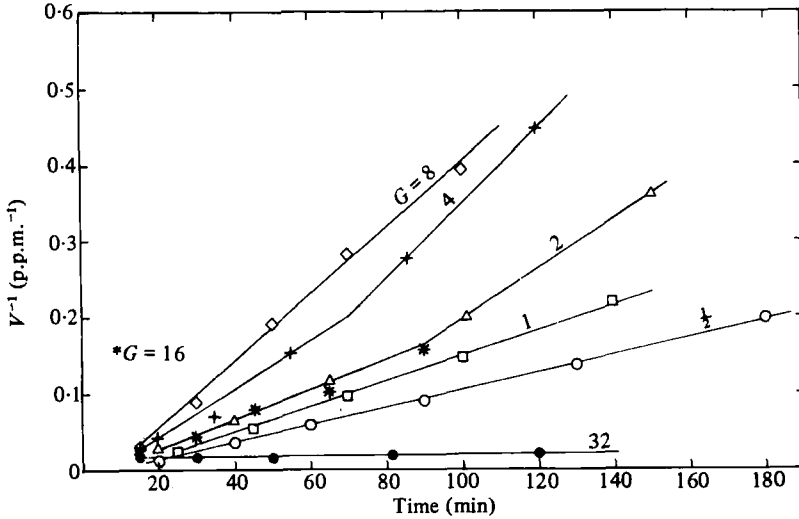


FIGURE 6. Inverse total suspended-particle volume during illite experiments at shear rates of 0.5, 1, 2, 4, 8, 16 and 32 s<sup>-1</sup>.

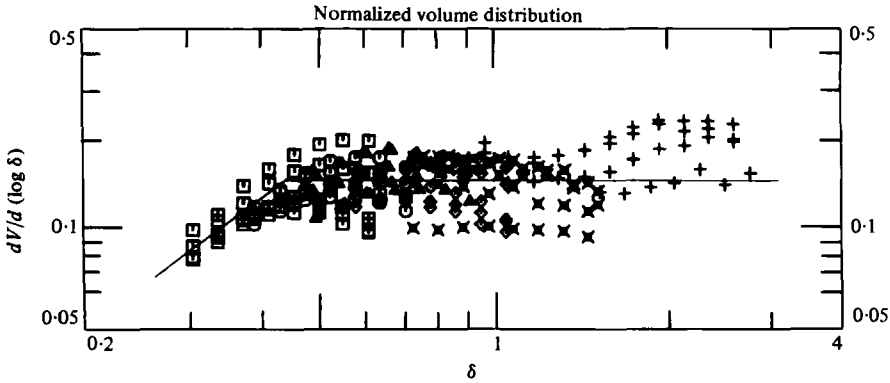


FIGURE 7. Normalized volume distributions for illite at  $G = 0.5$  ( $\square$ ), 1 ( $\circ$ ), 2 ( $\triangle$ ), 4 ( $\diamond$ ), 8 ( $\times$ ) and 16 s<sup>-1</sup> (+).

could not be normalized because there was no decrease in total suspended volume. The dimensionless constants characterizing illite coagulation in seawater were  $A_b = 0.10$  and  $A_{sh} = 0.021$ .

*Discussion*

This discussion compares the assumptions necessary in the derivation of coagulating particle-size distributions with the experimental results for clay particles in artificial seawater.

The first assumption was the existence of a particle-size distribution in local equilibrium, maintained by a flux of particle volume through the size distribution. Experimentally, a constant flux of small particles into the distribution could not be imposed while maintaining a known rate of laminar fluid shear. Instead, batch experiments were conducted and decaying self-similar particle-size distributions were

observed. The second assumption required the dominance of only one coagulation mechanism at a given size. Experimental results indicate that the assumption is reasonable for Brownian and shear coagulation. A transition region between the mechanisms exists and is probably less than a factor of two in diameter. The dominant contribution to the volume flux through the size distribution appears to be determined by collisions between particles comparable in size.

The concentration of ions in artificial seawater was sufficient to destabilize kaolinite and illite clay particles. For kaolinite the normalized diameter separating Brownian and shear coagulation occurred at  $\delta = 0.9$ , while for illite the separation was at  $\delta = 0.44$ . The dimensionless coagulation constants for kaolinite and illite were different, along with the volume removal-rate constant at a given shear rate. Also, illite aggregates were more susceptible to aggregate breakup at higher fluid shear rates. These differences between kaolinite and illite coagulation results have been qualitatively related to the higher porosity of illite clay aggregates in seawater (Hunt 1980*a*).

The last assumption was that the coagulation mechanisms could be represented by characteristic parameters of the collision mechanisms. The choice of  $G$  to characterize shear coagulation was shown to be valid, and the choice of  $kT/\mu$  for Brownian coagulation appears to be reasonable, although experiments were conducted only at room temperature. In the specification of particle volume flux through the distribution and identification of characteristic parameters for coagulation, aggregate density was implicitly assumed to be independent of particle size. For the experimental data collected over the narrow range of 0.6 to about  $1.2\ \mu\text{m}$  equivalent spherical diameter, the assumption of uniform aggregate density is probably reasonable. Experimental evidence indicates that aggregate density decreases with increasing aggregate diameter over the range  $1\text{--}2000\ \mu\text{m}$  (McCave 1975; Tambo & Watanabe 1979).

Preliminary experiments were conducted with dilute oil-in-water emulsions to avoid the problems of aggregate breakup during counting and aggregate density variations with size. For simple oil-in-water emulsions, mechanically dispersed in high-ionic-strength solutions, the oil droplets were not completely destabilized, and the results could not be used for testing the coagulation size-distribution predictions (Hunt 1980*a*).

## 6. Conclusions

Predictions of coagulating particle-size distributions were obtained by dimensional analysis, following techniques developed for analysis of aerosol dynamics and small-scale velocity and scalar fluctuations in turbulent fluids. Considerable simplification of the coagulation mechanisms was necessary, and the predictions apply only after a local equilibrium has developed in the size distribution. The predicted size distributions for Brownian and shear coagulation were verified with clay particles destabilized in artificial seawater. Measured particle-size distributions were in agreement with the predicted dependence on diameter, fluid shear rate and particle volume flux through the distribution. Because larger aggregates could not be sized, the prediction for differential-sedimentation coagulation was not tested.

The dimensional-analysis approach is a simple and quantitative technique for describing coagulation in continuous particle-size distributions. Only a single dimensionless constant is required to characterize each coagulation mechanism. The

experimental results for kaolinite and illite clays indicate that the dimensionless constants are a function of particle surface chemistry and probably a function of the ionic composition of the destabilizing solution. At this time the dimensionless constants must be determined experimentally, but once obtained they allow a far more convenient analysis of coagulation after sufficient time than a formal solution to (1.2).

The verified predictions for Brownian and shear coagulation of clay particles have direct application to clay-particle removal from seawater. The results have possible application to other natural waters and particle-separation processes, where information is required on particle-size distributions and total suspended volume removal rates. A number of important particle-fluid interactions were not considered, including aggregate breakup by fluid shear and coagulation in turbulent fluids containing a distribution of local shear rates. The understanding of coagulation gained in this work provides a theoretical and experimental framework for considering other mechanisms and flow regimes.

The author thanks the following organizations for their financial support of this work: United States Environmental Protection Agency, Union Oil Company, Jessie Smith Noyes Foundation Inc. and United States National Oceanographic and Atmospheric Administration, Office of Sea Grant (NA80AA-D-00120). The work presented here is from material submitted in a doctoral thesis by the author to the California Institute of Technology, Pasadena. During the course of this research the author received helpful advice from James J. Morgan and E. John List. The author also appreciates the detailed reviews this paper received by the referees.

#### REFERENCES

- ADLER, P. M. 1981 Heterocoagulation in shear flow. *J. Colloid Interface Sci.* **83**, 106-115.
- BATCHELOR, G. K. 1953 *The Theory of Homogeneous Turbulence*. Cambridge University Press.
- BATCHELOR, G. K. 1959 Small-scale variation of convected quantities like temperature in turbulent fluid. Part 1. General discussion and the case of small conductivity. *J. Fluid Mech.* **5**, 113-133.
- BIRKNER, F. B. & MORGAN, J. J. 1968 Polymer flocculation kinetics of dilute colloidal suspensions. *J. Am. Water Works Assoc.* **60**, 175-191.
- DRAKE, R. L. 1976 Similarity solutions for homogeneous and nonhomogeneous aerosol balance equations. *J. Colloid Interface Sci.* **57**, 411-423.
- EDZWALD, J. K., UPCHURCH, J. B. & O'MELIA, C. R. 1974 Coagulation in estuaries. *Environ. Sci. Technol.* **8**, 58-63.
- FRIEDLANDER, S. K. 1960a On the particle-size spectrum of atmospheric aerosols. *J. Met.* **17**, 373-374.
- FRIEDLANDER, S. K. 1960b Similarity considerations for the particle-size spectrum of a coagulating, sedimenting aerosol. *J. Met.* **17**, 479-483.
- FRIEDLANDER, S. K. 1977 *Smoke, Dust and Haze: Fundamentals of Aerosol Behaviour*. Wiley-Interscience.
- GELBARD, F. & SEINFELD, J. H. 1979 The general dynamic equation for aerosols, theory and application to aerosol formation and growth. *J. Colloid Interface Sci.* **68**, 363-382.
- HONIG, E. P., ROEBERSEN, G. J. & WIERSEMA, P. H. 1971 Effect of hydrodynamic interaction on the coagulation rate of hydrophobic colloids. *J. Colloid Interface Sci.* **36**, 97-109.
- HUNT, J. R. 1980a Coagulation in continuous particle size distributions; theory and experimental verification. Ph.D. thesis, California Institute of Technology, Pasadena (Rep. no. AC-5-80, *W. M. Keck Laboratory of Environmental Engineering Science, California Institute of Technology*).

- HUNT, J. R. 1980b Prediction of oceanic particle size distributions from coagulation and sedimentation mechanisms. *Adv. Chem. Ser.* **189**, 243-257.
- JEFFREY, D. J. 1981 Quasi-stationary approximations for the size distribution of aerosols. *J. Atmos. Sci.* **38**, 2440-2443.
- KERR, P. F. *et al.* 1949-50 *Reference Clay Minerals: Am. Petroleum Inst. Res. Proj.* **49**. Preliminary Rep. nos. 1-8. Columbia University.
- LAWLER, D. F., O'MELIA, C. R. & TOBIASON, J. E. 1980 Integral water treatment plant design: From particle size to plant performance. *Adv. Chem. Ser.* **189**, 353-388.
- LICHTENBELT, J. W. TH., PATHMAMANTHARAN, C. & WIERSEMA, P. H. 1974 Rapid coagulation of polystyrene latex in a stopped-flow spectrophotometer. *J. Colloid Interface Sci.* **49**, 281-285.
- MANLEY, R. ST. J. & MASON, S. G. 1955 Particle motions in sheared suspensions. III. Further observations on collisions of spheres. *Can. J. Chem.* **33**, 763-773.
- MASON, B. J. 1971 *Physics of Clouds*, 2nd edn. Clarendon.
- McCAVE, I. N. 1975 Vertical flux of particles in the ocean. *Deep-Sea Res.* **22**, 491-502.
- OVERBEEK, N. TH. G. 1977 Recent developments in understanding of colloid stability. *J. Colloid Interface Sci.* **58**, 408-422.
- PRUPPACHER, H. R. & KLETT, J. D. 1978 *Microphysics of Clouds and Precipitation*. Reidel.
- PULVERMACHER, B. & RUCKENSTEIN, E. 1974 Similarity solutions of population balances. *J. Colloid Interface Sci.* **46**, 428-436.
- RILEY, J. P. & SKIRROW, G. 1965 *Chemical Oceanography*, vol. 1. Academic.
- SMOLUCHOWSKI, M. 1917 Versuch einer mathematischen Theorie der Koagulationkinetik kolloider Lösungen. *Ann. Physik. Chem.* **92**, 129-168.
- SPIELMAN, L. A. 1970 Viscous interactions in Brownian coagulation. *J. Colloid Interface Sci.* **33**, 562-571.
- SPIELMAN, L. A. 1977 Particle capture from low-speed laminar flows. *A. Rev. Fluid Mech.* **9**, 297-319.
- SWIFT, D. L. & FRIEDLANDER, S. K. 1964 The coagulation of hydrosols by Brownian motion and laminar shear flow. *J. Colloid Sci.* **19**, 621-647.
- TAMBO, N. & WATANABE, Y. 1979 Physical characteristics of flocs - I. The floc density function and aluminum floc. *Water Res.* **13**, 409-419.
- TAYLOR, G. I. 1936 Fluid friction between rotating cylinders. Part I. Torque measurements. *Proc. R. Soc. Lond. A* **157**, 546-564.
- VAN DE VEN, T. G. M. & MASON, S. G. 1977 The microrheology of colloidal dispersions VII. Orthokinetic doublet formation of spheres. *Colloid Polym. Sci.* **255**, 468-479.
- VAN OLFPHEN, H. 1977 *An Introduction to Clay Colloid Chemistry*, 2nd edn. Wiley-Interscience.
- WANG, C. S. & FRIEDLANDER, S. K. 1967 The self-preserving particle size distribution for coagulation by Brownian motion. II. Small particle slip correction and simultaneous shear flow. *J. Colloid Interface Sci.* **24**, 170-179.
- ZEICHNER, G. R. & SCHOWALTER, W. R. 1977 Use of trajectory analysis to study stability of colloidal dispersions in flow fields. *A.I.Ch.E. J.* **23**, 243-254.